Strength Testing and Material Characterization of Cactus Spines

A Senior Project

presented to

the Faculty of the Materials Engineering Department

California Polytechnic State University, San Luis Obispo

In Partial Fulfillment

of the Requirements for the Degree

Bachelor of Science, Materials Engineering

by

Mary Cooper, Jeff Goldstein, Tom Tarlton

June 2013

Approval Page

Project Title: Strength Testing and Material Characterization of Cactus Spines

Authors: Mary Cooper, Jeff Goldstein, Tom Tarlton

Date Submitted: June 7, 2013

CAL POLY STATE UNIVERSITY
Materials Engineering Department

Since this project is a result of a class assignment, it has been graded and accepted as fulfillment of the course requirements. Acceptance does not imply technical accuracy or reliability. Any use of the information in this report, including numerical data, is done at the risk of the user. These risks may include catastrophic failure of the device or infringement of patent or copyright laws. The students, faculty, and staff of Cal Poly State University, San Luis Obispo cannot be held liable for any misuse of the project.

Prof. Trevor Harding
Faculty Advisor

_____
Signature

Prof. Richard Savage
Department Chair

_____
Signature

Acknowledgements

We would like to acknowledge our project advisor, Dr. Trevor Harding, for all of his guidance and support while working on this project. Additionally, we would like to thank Dr. Blair London for his help with mechanical testing and Will Hilgenberg for his help in the machine shop.

Table of Contents

List of Tables

List of Figures

Abstract

Twelve different species of cactus spines from 6 different genera were collected from living specimens and maintained in a dry storage environment. Spines from each species underwent 3-point bend testing, XRD testing, and SEM imaging. XRD analysis was used to verify the presence of cellulose whisker like nanocrystals and to calculate the percent crystallinity of each spine. SEM images were captured of fracture surfaces at viewing angles of 90˚ and 45˚ relative to the fracture surface, with magnifications ranging between 150x and 4,000x. A total of six spines from each species were tested in three point bending using a high-resolution load cell. The elastic modulus and fracture strength varies between species and between individual spines within a species. The 12 species can be separated into 3 different flexural strength categories. The high, medium, and low strength spine categories demonstrate differences in percent crystallinity and fiber size. The percent crystallinity ranged from 48.0% to 76.3%, with higher crystallinities exhibited in the stronger spines. Every XRD scan exhibited a crystalline peak at 22.7˚, confirming the expected presence of cellulose I within the spines. Fiber size within the spines ranged from 2.9 to 10.0 microns, with little in surface texture and spine structure.

Keywords: Cactus spines, strength testing, percent crystallinity, biocomposite, biomimicry, materials engineering.

Introduction

With a current need for sustainable manufacturing practices within the global economy, the ability to mimic natural structures for future engineering design is slowly developing into a crucial aspect of environmentally sustainable engineering. Since cactus spines have an extremely high specific strength and stiffness, they provide one potential candidate for a biocomposite structure; however, the mechanical properties and underlying structure of cactus spines are relatively unexplained in current literature. Additionally, the variation in structure between different species of cacti is unknown.

The structure of a cactus spine is a unique composite that consists of roughly 50% cellulose and 50% arabinan[1]. This structure varies from other organic plant materials, such as wood, which consists of roughly 50% cellulose, 25% lignin, and 25% non-structural polysaccharides[2]. Due to this difference, several previous studies have examined the spines of *Opuntia ficus-indica*[1,2] with varying conclusions. The *O. ficus-indica* spines produced high strength values under three point bending[2] (Table I).

Table I. Mechanical Properties of *Opuntia ficus-indica*

Spine	**Average Modulus of Elasticity**	**Average Bending Strength**
Green (Fresh)	28.0 ± 3.66 GPa	609 ± 48.1 MPa
Dry	33.5 ± 5.15 GPa	779 ± 87.7 MPa

The modulus values demonstrated by *O. ficus-indica* are greater than several composite materials (Carbon fiber reinforced polycarbonate (13 GPa)[3] but less than an individual E-glass fiber (72 GPa)[3]. This is an impressive comparison considering the spines are a natural material that are not refined in any way to reduce impurities or defects. With these material properties, the structure of the spines may be mimicked in order to create a biocomposite.

Experimental Procedure

All spines were harvested from the cactus specimens with clipping shears, clipped as close to the cactus surface as possible. The spines were stored in a cool, arid storage location

until needed for examination. None of the spines were experimentally dried using a furnace, so they are assumed to be in the green condition.

3 Point Bend Testing

With regard to mechanical testing, data collection for each species was as standardized as possible. All spines were in the as-harvested condition for testing and were not trimmed in length. Width and thickness measurements were taken at the midpoint of the spine where the crosshead made contact. ASTM D790-10[4] is designed for the purposes of testing plastics in the 3-point bend method.

The span width was set to create an overhang of at least 10% of the length of the spine over each edge. Spines were laid over the span concave up to limit the possibility of rolling and slipping. The method specified a 1 mm/min crosshead speed, with a data point to be taken every half second. Spines were tested until a fracture resulting in 40% strength loss or greater. All data points were recorded in the .RAW file format. Flexural stress was treated as a straight maximum from the outputs of the formula. Modulus of elasticity was obtained as the maximum value obtained after disregarding the first 50 data points, when the data reached a more constant slope. The calculated data was input to Minitab statistical software to compare the data through One-Way ANOVA testing.

The 3-point bend method was chosen over a 4 point bend method due to the replication of a more natural bending mode and a decreased tendency to bring out structural aberrations in the material. Preliminary testing determined shifting and rolling to be a non-issue in all spines exceeding 25mm. However, over the course of this project, 5 of the 12 species tested were below the requisite size for testing on the 3 point fixture owned by the Cal Poly Materials Engineering Department. As such a smaller rig was devised and manufactured to be able to test spines as small as 8mm long. Although an ASTM standard was not found for materials shorter than 25mm in length, testing proceeded according to ASTM D790-10 in all other regards.

XRD Testing

X-Ray Diffraction (XRD) testing was done using a Siemens D5000 diffractor. Each spine tested was mounted onto a slide using silly putty. The spine was leveled to the surface plane of the slide and placed into the diffractor. The scan speed of the diffractor was set to 1°/minute in 0.1 increments. The Bragg's angle (2θ) range of the scan was 10° - 35°.

Once the scanning was complete, the resulting graph was uploaded to EVA 3.0, the Bruker Analytical X-Ray Systems evaluator. The pattern of the graph was then compared to EVA's pattern database to confirm the presence of cellulose I.

DSC Testing

Differential Scanning Calorimetry (DSC) was conducted using an Exstar 6000 calorimeter in an attempt to further characterize the crystallinity of the spine samples. Three species were selected for analysis, and the spines were fractured into small pieces (~ 1 mm) and analyzed with a heating/cooling rate of 10°C/min. The temperature range for the spines was between 20°C and 500°C.

Electron Microscopy

The spines were imaged using an FEI Quanta 200 scanning electron microscope (SEM). Prior to SEM analysis, each spine was submerged in liquid nitrogen for 2 minutes and bent until fracture using two pairs of pliers. Both halves of a fractured spine would be placed on the SEM stage, with one half being vertically oriented and the other at a 45° angle to the horizontal (Figure 1).

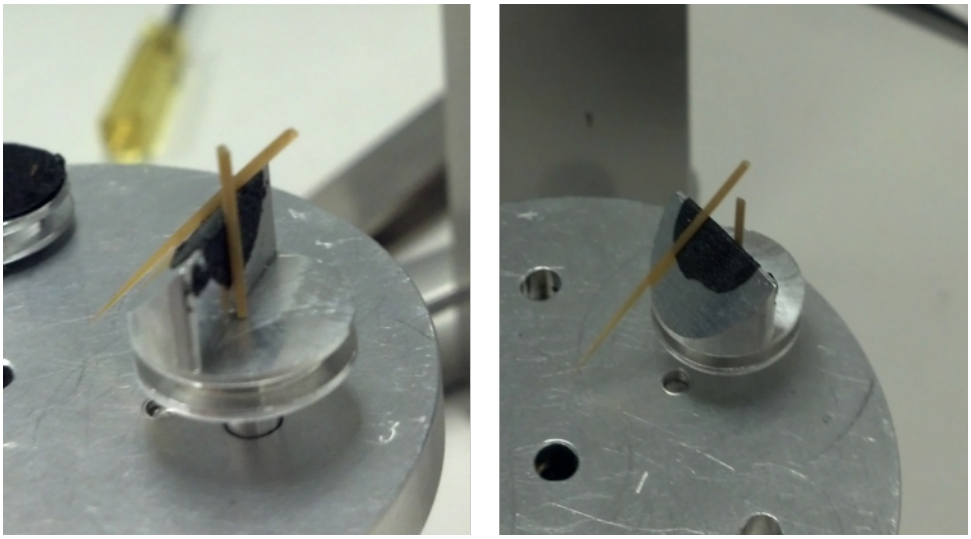

(*a*) (*b*)

Figure 1. (*a)* The SEM stage used for orienting the cactus spines under the electron beam, with one spine being held 90 degrees and one spine held 45 degrees to the horizontal. *(b)* The backside of the SEM stage with a 45° slope for the spine.

Once the spine halves were prepared for SEM imaging, the spines were viewed under low vacuum conditions with a spot size of 3.5 and a voltage of 20kV. Each spine orientation (cross sectional and 45° angle to the horizontal) had an image captured at 300x and 2000x magnification, for a total of at least 4 images for each of the 15 species. Additional magnifications were used to examine the spine, with any useful images being stored in addition to the standard 4 images for each spine.

Results

Mechanical Testing

Mechanical testing of approximately 70 samples produced load (N) versus extension (mm) graphs for each of the 12 species tested. All calculations were made using the assumption of a rectangular cross-section. The collected data was used to find flexural strength (σ_f) and tangential modulus of elasticity (E_b). The equation for flexural strength is as follows:

$$\sigma_f = \frac{3PL}{2bd^2} \qquad (1)$$

where P is the load at a given point on the load deflection curve
L is the support span
b is the beam width
d is the depth

The equation for the tangential modulus of elasticity is as follows:

$$E_b = \frac{L^3 m}{4bd^3} \qquad (2)$$

where m is the initial slope of the tangent of the load/deflection curve.

Using these equations, the collected data was used to calculate mechanical properties such as flexural strength (Figures 2 & 3) and elastic modulus (Figure 4). Spines were tested to failure in all cases except for *S. crispatus,* which was tested to the limits of the fixture. Deflection exceeded 8mm in all cases and the graph showed load-bearing ability dropping as a result of

testing. Although the spine itself did not suffer any apparent fracture, the loading capacity dropped to almost half the maximum load between the 2mm mark and the 8mm mark, indicating internal fracture that was not readily visible.

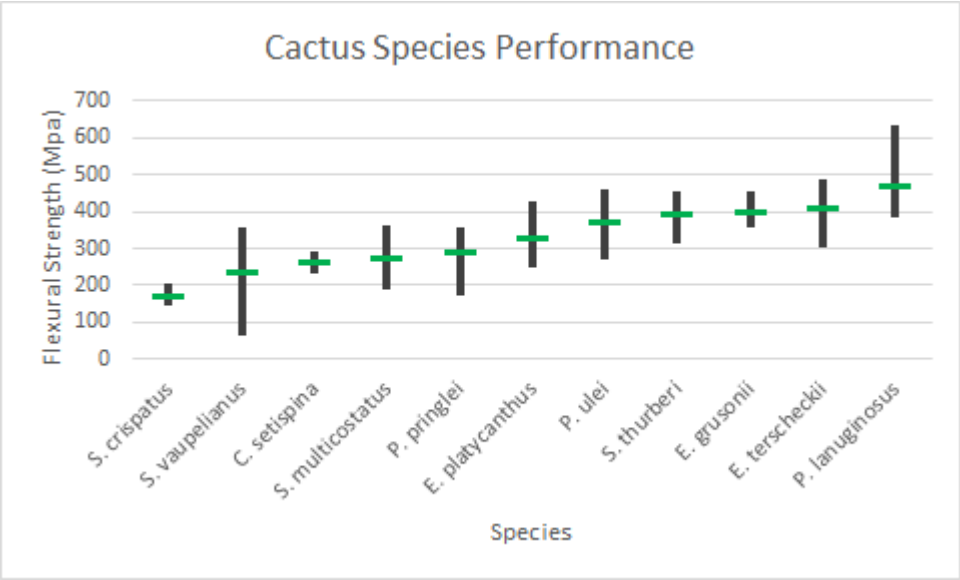

Figure 2. Mechanical testing data showing the average flexural strength of the tested species both as a range and as an average. Species were arranged in hierarchical order by average to give an idea as to different tiers of strength.

Since *P. pachycladus* significantly outperformed all other spines in flexural strength, its data was excluded from Figure 2. With *P. pachycladus* included in the data, all other spines are dwarfed by its performance (Figure 3). Even the lowest calculated value for *P. pachycladus* exceeds the highest calculated value for *P. lanuginosus* by more than 400 MPa; the data for *P. pachycladus* reaches a minimum strength of 900 MPa, with the strongest value exceeding 2000 MPa.

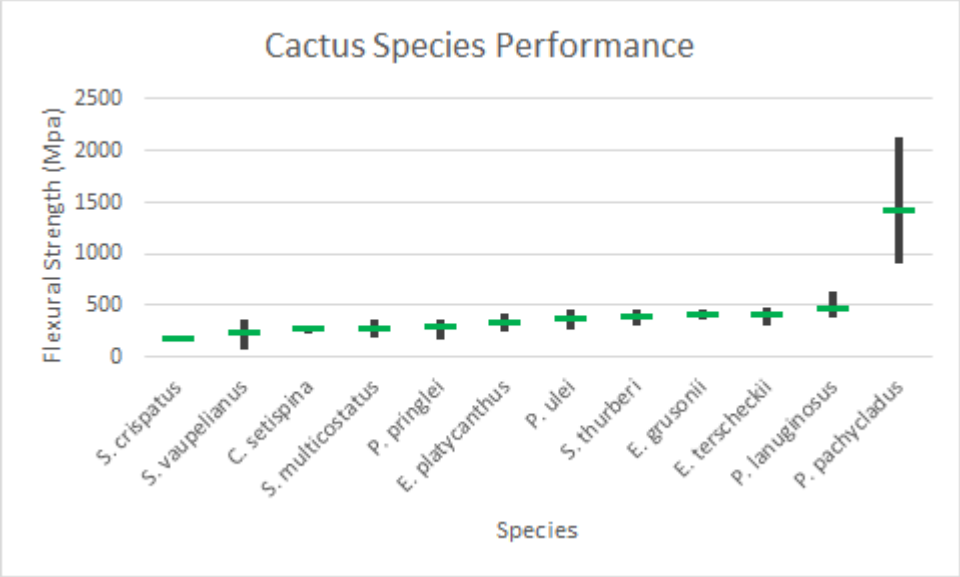

Figure 3. Mechanical testing data showing a comparison of *P. pachycladus* with the entire population of cactus spines.

Modulus of elasticity for the spines contains much more overlap between different species (Figure 4). *P. pachycladus* performs within a range similar to the other species, suggesting that its high strength values do not rely on an increased modulus.

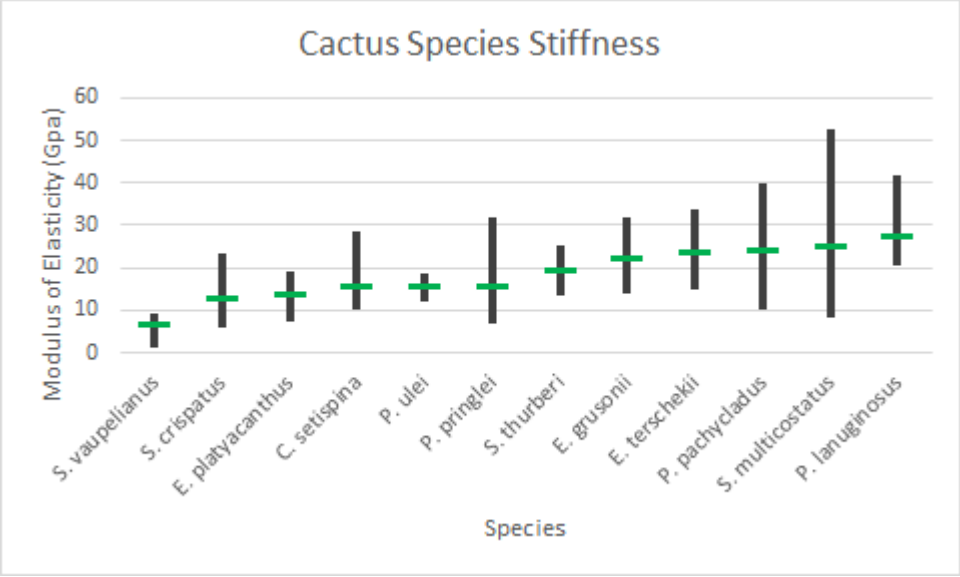

Figure 4. Mechanical testing data supporting assumption that all spines selected for initial testing fall into the category of high stiffness.

Spine Crystallinity

XRD testing produced an intensity plot for each spine (Figures 5 & 6). The peak patterns on this graph act as a fingerprint for the spines, with each peak indicating a different structure within the spine. All spines had crystalline peaks at 2θ's of ~14.5°, ~16.8°, and ~22.5°, which is the peak pattern for cellulose I. However, each spine possessed different intensities at these 2θ's, giving the spines individuality. The intensity of the amorphous peak for each spine also differed. These differences in intensities produce differences in percent crystallinities.

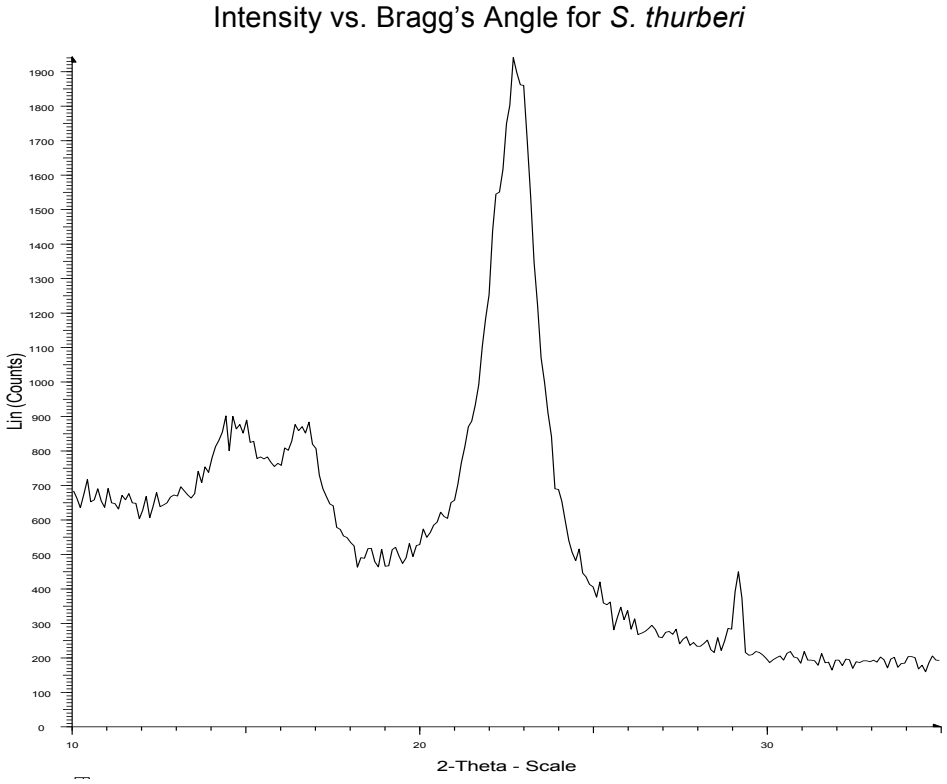

Figure 5. An XRD graph showing the "fingerprint" of the high percent crystallinity *S. thurberi* spine.

To illustrate the differences in XRD graphs between different species, it is useful to compare the intensities found in Figure 5 with those found in Figure 6. *S. thurberi* produces a crystalline peak with an intensity of 1900 counts while *S. multicostatus* produces the same peak with an intensity around 500 counts.

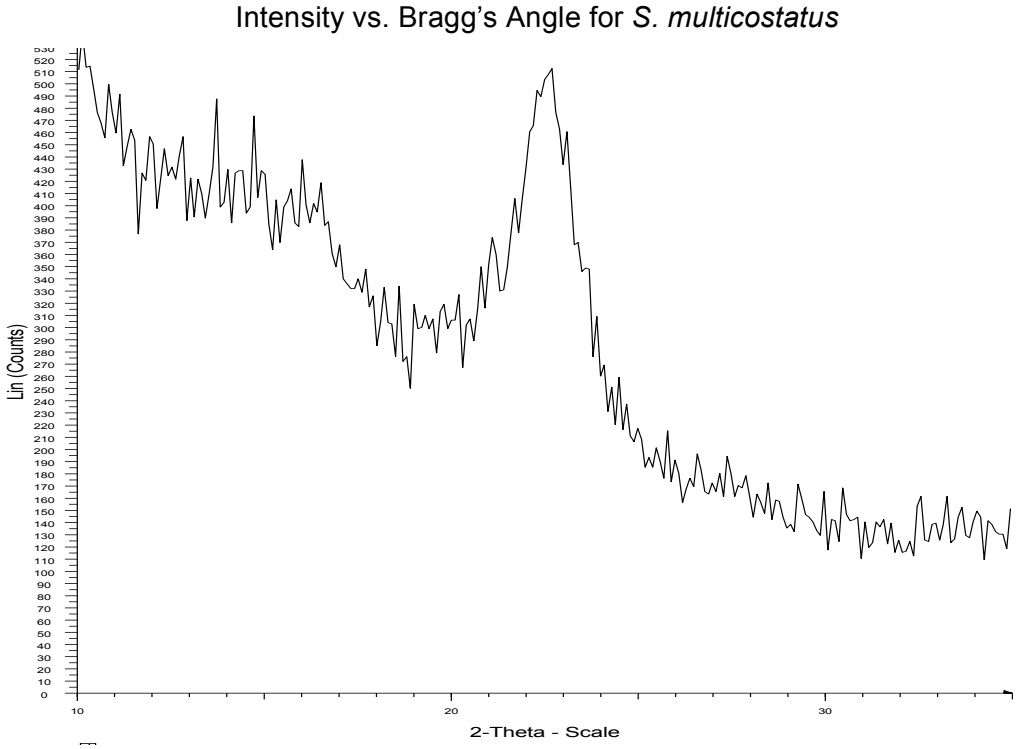

Figure 6. An XRD graph showing the "fingerprint" of the low percent crystallinity *S. multicostatus* spine.

To determine percent crystallinity of each spine, Segal's Ratio of Intensities[5] was used (eq. 3),

$$\%\, crystallinity = \frac{I_{200} - I_{am}}{I_{200}}\, X\, 100 \qquad \textit{eq 3}$$

where I_{200} is the crystalline intensity and I_{am} is the amorphous intensity. I_{am} for cellulose I is found at a 2θ of ~18.0° and I_{200} is found at a 2θ of ~22.5° (Figure 7).

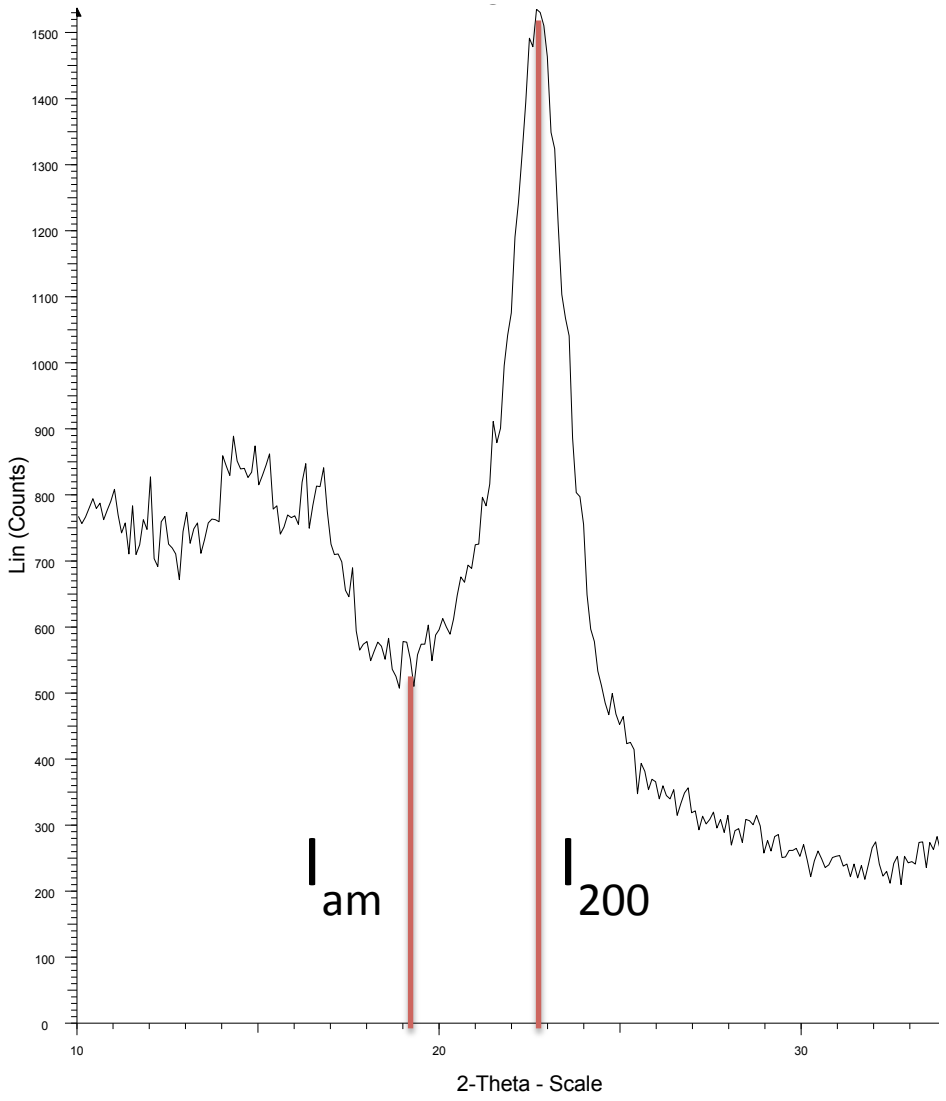

Figure 7. An XRD graph showing the amorphous intensity value (I_{am}) and the crystalline intensity value (I_{200}). The intensity of these two peaks is compared in order to calculate the percent crystallinity of each spine.

The XRD graphs of each spine tested were used to find an average percent crystallinity for each species (Table II). The percent crystallinities of the species ranged from 48.0% to 76.3%.

Table II. Percent Crystallinities of Twelve Cactus Spine Species

Spine Species	% Crystallinity
Myrtillocactus geometrizans	48
Stenocactus multicostatus	51.4
Echinocactus platyacanthus	53.4
Echinocactus grusonii	54.7
Stenocactus vaupelianus	57.6
Stenocactus crispatus	64.7
Pachycereus pringlei	65.6
Pilosocereus languinosus	72.9
Pilosocereus ulei	75.8
Echinopsis terscheckii	75.9
Pilosocereus pachycladus	75.9
Stenocactus thurberi	76.3

To complement the XRD testing, an attempt at DSC testing was used to determine enthalpies of crystallization; however, the DSC plot for a cactus spine provided several interesting features whose meaning is not immediately clear (Figure 8).

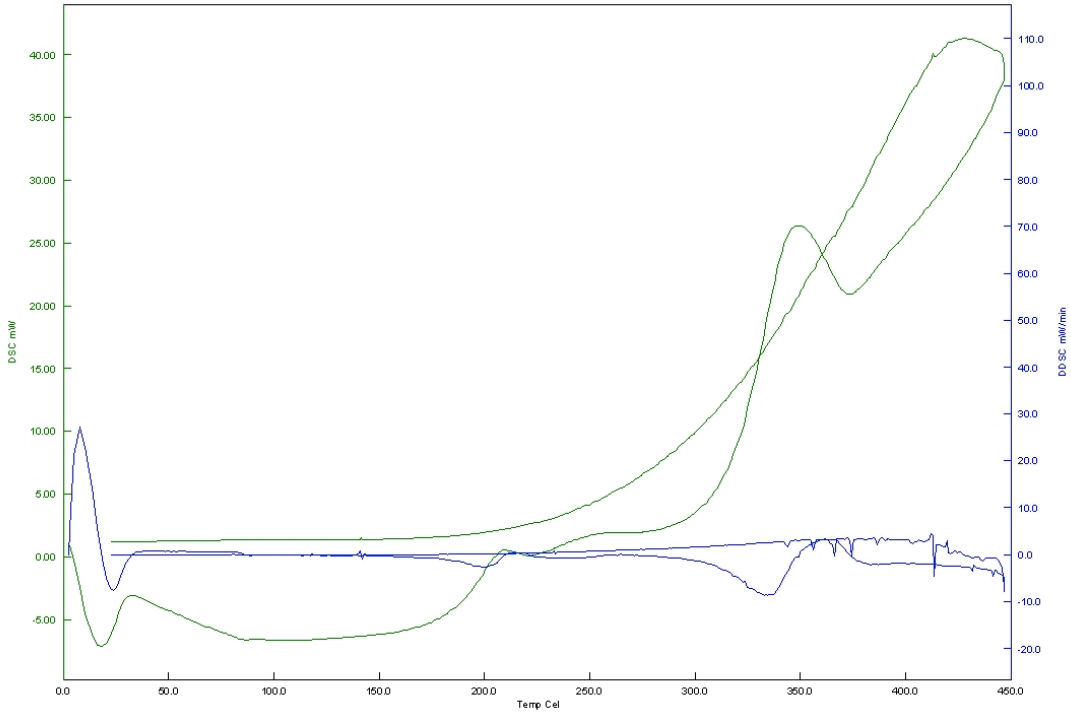

Figure 8. A DSC plot for *E. terscheckii* that cycles from 20°C to 450°C with a heating and cooling rate of 10°C/min.

On heating, the cactus spine appears to experience an endothermic reaction between 25°C and 200°C, meaning the cactus spine is absorbing energy. This occurs again at approximately 375°C, after a large exothermic reaction has occurred. Either endothermic reaction could indicate recrystallization, but the higher temperature seems more likely due to increased energy. At this point, the remaining non-crystalline cellulose could gain enough energy to crystallize, creating a 100% crystalline material. Interestingly, the same activity is not experienced on cooling, indicating that a sort of annealing has occurred in the spine[*].

Spine Structure

The SEM analysis of the cactus spines provided images of the microscopic physical structure as well as an accurate way to measure spine dimensions such as spine diameter and fiber diameter (Appendix B). One of the most pronounced features present in all of the spines is the presence of a microscopic substructure within the spine. An individual cactus spine seems to consist of a group of fibers bound together to form the cellulose-arabinan composite (Figure 8).

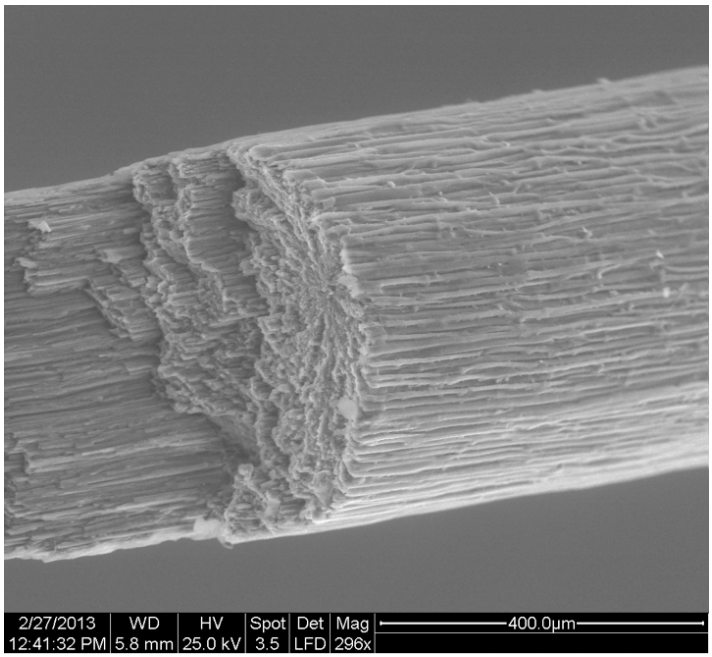

Figure 9. A fractured spine of *Pachycereus pringlei* is shown under low magnification, exhibiting the continuous fiber structure on the exterior of the spine.

[*] DSC testing was sought as a confirmation for XRD results at the latter end of this project. The analysis is speculative and further research and testing is needed to properly validate the DSC plot explanation.

When the fracture surface of one fiber is magnified, it appears that many smaller sub-fibers comprise the larger fiber (Figure 9).

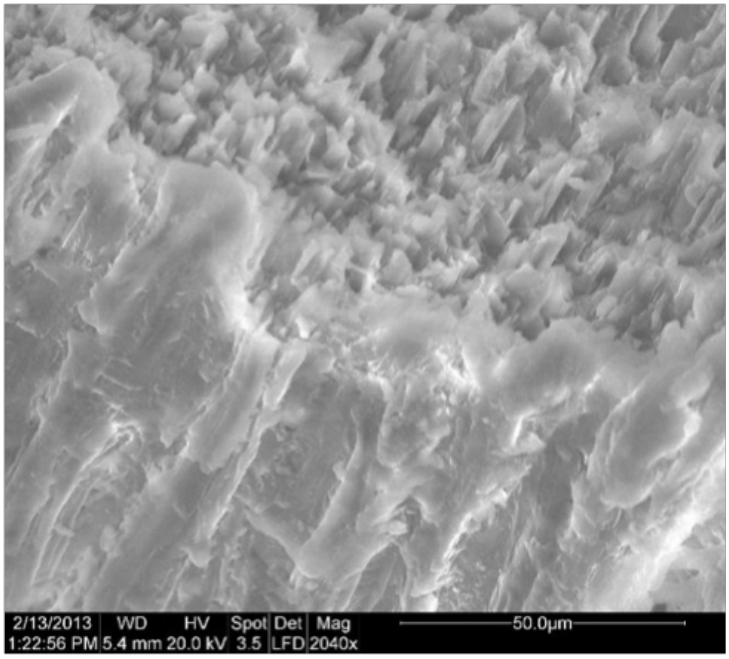

Figure 10. The fracture surface edge of *Echinocactus platyacanthus* demonstrates that the skin fibers (bottom half of image) appear to be made of many smaller sub-fibers (top half of image).

When the cross section of the fracture surface is viewed (as if looking down the length of the spine), the individual fiber cross sections can be seen; however, these fibers do not appear to be circular (Figure 10). All of the spines' fibers exhibited a non-uniform cross section that seemed to interlock with each other.

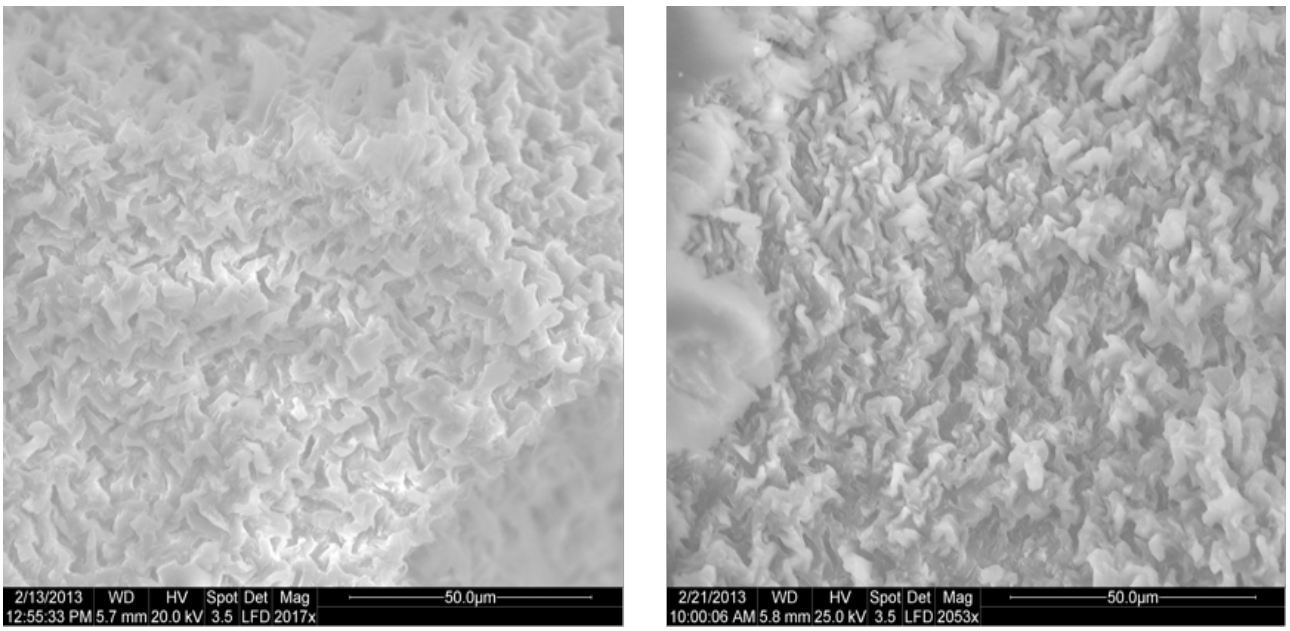

(a) *(b)*

Figure 11. *Echinocactus platyacanthus* (a) and *Stenocactus crispatus* (b) are two examples of the non-uniform fiber cross sections found in the cactus spines.

In addition to examining external structure, the SEM images provided data measuring the spine diameter as well as the fiber diameter. The spine diameters ranged from .3 mm to 2.7 mm and the fibers ranged from 2.9 µm to 16.3 µm (as measured from the external skin of the spine viewed at 45° to the horizontal) (Appendix B).

Discussion

Since this project was one of the first scholastic attempts at researching the mechanical properties of cactus spines, this project may have raised more questions than it answered.

All of the spines tested in this research were chosen as specimens because they had similar characteristics at the most primitive level (i.e. they had similarities that were visible with the naked eye). This is because the research scope needed to be narrowed to fit the span of the project timeline. With all of the cacti species that exist in the world, it would have been too large of a task to try and create test jigs and procedures for all of the different examples of cactus spines that exist. Aside from the stiff, lance-like spines that were chosen for this project, hundreds of other spines exist that demonstrate numerous variations that would not have been

easily testable with the procedure used in this project. With this in mind, it is no surprise that the spines examined demonstrate numerous similarities.

The mechanical testing has proven that there are differences in modulus of elasticity and flexural strength amongst different species of cactus spines. Since some species are much stronger than others, the answer must exist in the structural properties, although it may not be due to one specific characteristic. There does not appear to be a correlation between percent crystallinity and flexural strength (Figure 12); however, it is interesting to note that the spines with the highest four percent crystallinities are also spines that have flexural strengths in the top five of all spines tested. The addition of more species' strength data could prove that the spines in this study are similarly strong (and strong compared to many other cactus spines) and have a high percent crystallinity, but more data is needed to support that idea.

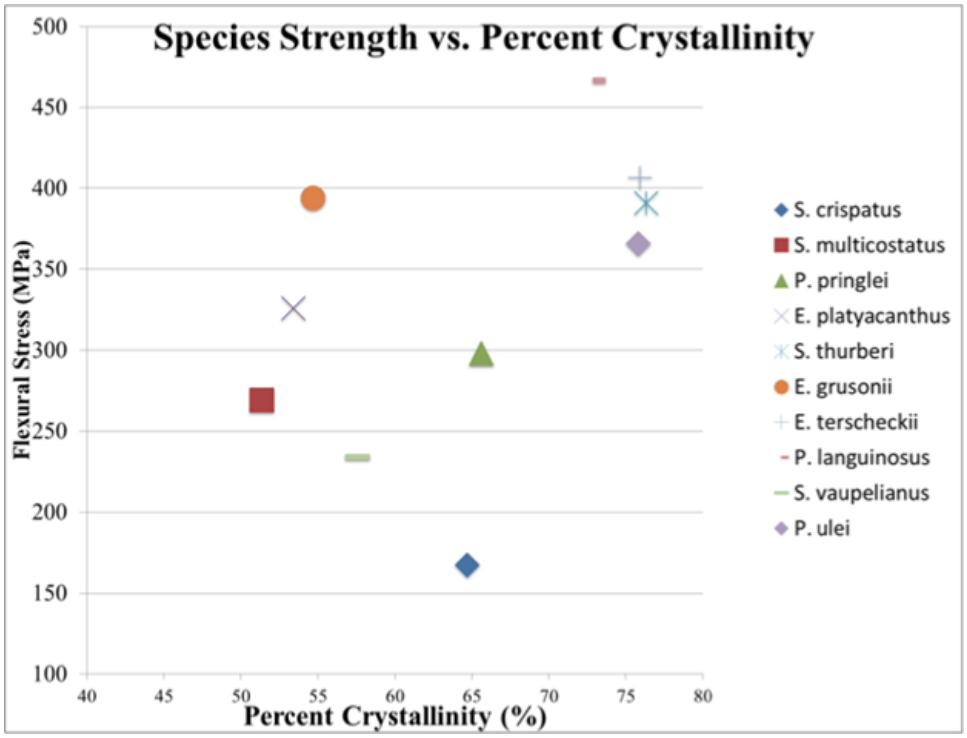

Figure 12. As demonstrated in this plot of flexural stress vs. percent crystallinity, there is no correlation between percent crystallinity of the spines and flexural stress.

When comparing the strengths and physical properties of the spines, all of the spines seemed to have a similar physical structure with little correlation between physical properties and strength. Each spine consisted of a bundled structure of smaller sub-fibers, but each sub-fiber appeared to have a non-circular cross section when viewed from above (Figure 11). This non-circular cross section appears on the fracture surface but is not guaranteed to exist

internally on a non-fractured spine. While this option is not likely due to the interlocking pattern of the sub-fibers, it is important to note that this non-circular pattern may have been formed during the fracture process.

For each spine tested, spine size and shape varied widely both within species and between species. Although the base geometries were approximately the same, species thickness, length, and width all suffered from natural variation. The assumption of a rectangular cross section was made for all spines. Although this assumption may have resulted in unusually low strength and stiffness values, by assuming extra material presence, the variance of the cross section was no more circular than rectangular. To further refine bend test data for each spine, research into the testing of non-rectangular beam shape would be necessary, taking into account the different moment of inertias present in non-uniform shapes.

One possible explanation for strength variation between species is the different surface textures of the spines. When viewed under SEM, several spines had a non-continuous fiber pattern on the surface, meaning that the fibers did not run the entire length of the spine. Upon relating these select spines to the strength data, the three spines fell in the high, medium, and low strength regions of the data. This implies that the surface texture has little effect on mechanical properties.

Since *P. pachycladus* maintained a flexural strength approximately 3 times higher than all other species but had a similar modulus of elasticity, it is worth discussing possible sources of error. The spines were tested on the same span as the *C. setispina* spines during the same lab session, indicating the equipment was operating normally. Calculations were also redone for the spines with no indication of previous error. Additional tests of *P. pachycladus* are highly recommended in future testing, since the current data seems to retain validity.

With respect to spine properties, the spine diameter, spine length, and fiber diameter were plotted against the percent crystallinity and mechanical properties. No correlation existed between the physical properties and mechanical properties. This would lead to the conclusion that the strength is determined by a property not discussed in this project, such as composite composition of arabinan and cellulose, or that our method of assessing spine properties was not sufficient in some way.

Conclusions

1. Flexural strength is statistically different at the 95% Confidence Interval between each species.
2. Modulus of elasticity is statistically different at the 95% Confidence Interval between each species.
3. A weak correlation exists between crystallinity and flexural strength. Addition of data from more species suggests a stronger correlation may be found with further research.
4. SEM images indicate a non-uniform fiber cross section made up of bundles of sub-fibers, which create the fiber composite matrix.
5. No obvious correlation is found between strength, percent crystallinity, and physical structure within this research.

References

1. Vignon, M.R., Heux, L., Malainine, M.E., and Mahrouz, M. “Arabinan-cellulose composite in *Opuntia ficus-indica* prickly pear spines,” *Carbohydrate Research.* 339, 123-331. (2004).

2. Gindl-Altmutter, W., and Keckes, J. “The structure and mechanical properties of spines from the cactus *Opuntia ficus-indica*,” *Bioresources.* 7, 1232-1237. (2012).

3. Smith, W., Hashemi, J. *Foundations of Materials Science and Engineering,* McGraw-Hill, New York. (2011).

4. ASTM Standard D790, 2010, "Standard Test Methods for Flexural Properties of Unreinforced and Reinforced Plastics and Electrical Insulating Materials," ASTM International, West Conshohocken, PA, 2010, DOI: 10.1520/D0790-10, www.astm.org.

5. Bansal, P., Hall, M., Realff, M.J., Lee, J.H., Bommarius, A.S. “Multivariate statistical analysis of X-ray data from cellulose: A new method to determine degree of crystallinity and predict hydrolysis rates,” *Bioresource Technology*. 101, 4461-4471. (2010).

Appendices

Appendix A. List of Examined Species

Genus	Species
Echinocactus	*platyacanthus*
Echinocactus	*grusonii*
Echinopsis	*terscheckii*
Myrtillocactus	*geometrizans*
Pachycereus	*pringlei*
Pilosocereus	*languinosus*
Pilosocereus	*ulei*
Pilosocereus	*pachycladus*
Stenocactus	*multicostatus*
Stenocactus	*vaupelianus*
Stenocactus	*crispatus*
Stenocactus	*thurberi*

Appendix B. Spine and Fiber Measurements

Species	**Fiber Diameter (µm)**	**Spine Length (mm)**	**Spine Cross Section Dimension 1 (mm)**	**Spine Cross Section Dimension 2 (mm)**
S. multicostatus	4.4	24	.83	.62
S. thurberi	5.1	27	.57	.57
P. lanuginosus	10	25	.75	.75
E. terscheckii	3.8	39	.7	.7
E. grusonii	7.1	35	1.7	1.2
S. crispatus	9.4	37	1.9	.45
P. pringlei	9.4	40	.52	.55
E. platyacanthus	2.9	36	1.6	1.4
F. viridescens	5.1	34	.66	2.7
M. geometrizans	5.9	23	1.5	1.2
P. leninghausii	15.4	20	.11	.11
P. ulei	16.3	19	.66	.55
P. pachycladus	6.3	17	.67	.67
S. vaupelianus	5.5	18	.42	.32